Ecological Modelling 221 (2010) 1348–1363

Contents lists available at ScienceDirect

Ecological Modelling

journal homepage: www.elsevier.com/locate/ecolmodel

Vegetation competition model for water and light limitation. I: Model description, one-dimensional competition and the influence of groundwater

R.J. Brolsma*, D. Karssenberg, M.F.P. Bierkens

Department of Physical Geography, Utrecht University, P.O. Box 80115, 3508TC Utrecht, The Netherlands

ARTICLE INFO

Article history:
Received 2 July 2009
Received in revised form 30 January 2010
Accepted 13 February 2010
Available online 19 March 2010

Keywords:
Eco-hydrology
Soil water
Vegetation
Growth
Groundwater
Modeling
Vegetation stress

ABSTRACT

Vegetation growth models often concentrate on the interaction of vegetation with soil moisture but usually omit the influence of groundwater. However the proximity of groundwater can have a profound effect on vegetation growth, because it strongly influences the spatial and temporal distribution of soil moisture and therefore water and oxygen stress of vegetation. In two papers we describe the behavior of a coupled vegetation–groundwater–soil water model including the competition for water and light. In this first paper we describe the vegetation model, compare the model to measured flux data and show the influence of water and light competition in one dimension. In the second paper we focus on the influence of lateral groundwater flow and spatial patterns along a hillslope. The vegetation model is based on a biophysical representation of the soil–plant–atmosphere continuum. Transpiration and stomatal conductance depend both on atmospheric forcing and soil moisture content. Carbon assimilation depends on environmental conditions, stomatal conductance and biochemical processes. Light competition is driven by tree height and water competition is driven by root water uptake and its water and oxygen stress reaction. The modeled and measured H_2O and CO_2 fluxes compare well to observations on both a diurnal and a yearly timescale. Using an upscaling procedure long simulation runs were performed. These show the importance of light competition in temperate forests: once a tree is established under slightly unfavorable soil moisture conditions it can not be outcompeted by smaller trees with better soil moisture uptake capabilities, both in dry as in wet conditions. Performing the long simulation runs with a background mortality rate reproduces realistic densities of wet and dry adapted tree species along a wet to dry gradient. These simulations show that the influence of groundwater is apparent for a large range of groundwater depths, by both capillary rise and water logging. They also show that species composition and biomass have a larger influence on the water balance in eco-hydrological systems than soil and groundwater alone.

1. Introduction

Within temperate climate zones vegetation growth is limited by water, light and nutrients. Especially in lowland areas in the temperate climate zone groundwater can have a profound effect on vegetation. This can occur indirectly through influence on the root-zone soil moisture content and directly if groundwater is present within the rootzone itself. Vegetation growth can be limited both as a result of a shortage as well as a surplus of soil moisture, causing either water or oxygen stress. However in most eco-hydrological modeling efforts thus far groundwater is not included (Rodriguez-Iturbe et al., 2007).

Our aim is to determine the influence of groundwater on vegetation dynamics and on the other hand show the effect of using an advanced vegetation model on the water fluxes in the hydrological system. In this series of two articles a model is introduced that is capable of simulating the coupled vegetation, soil water and groundwater dynamics in temperate climates including both water and oxygen stress of vegetation.

Vegetation growth models can be divided into two main groups: The first group consists of models that are based on the soil–plant–atmosphere continuum (SPAC) (e.g. Friend et al., 1997; Katul et al., 2003; Zavala, 2004; Daly et al., 2004). Carbon assimilation is simulated in a biophysical way, or at least using parameters and variables that have a physical meaning. Photosynthesis and root water uptake, as well as stomatal conductance are modeled explicitly in these models, while variation of ambient variables is taken into account. Due to computational demands these models normally run on a short timescale representing time series lasting at most a few days.

The second group are semi-empirical models (e.g. Parton, 1993; Running and Coughlan, 1988; Potter, 1993 that can run on a

* Corresponding author.
E-mail address: rbrolsma@gmail.com (R.J. Brolsma).

0304-3800/$ – see front matter © 2010 Elsevier B.V. All rights reserved.
doi:10.1016/j.ecolmodel.2010.02.012

time scale from days to centuries. Vegetation growth is usually modeled based on a maximum assimilation or growth rate that depends on species type, irradiance or is calculated using the model of Farquhar et al. (1980). This assimilation rate is then reduced based on empirical reduction functions for water, nutrients and temperature. This group includes the majority of forest growth models.

Although we are interested in long time series (up to a 1000 years) we chose to use a SPAC type approach, because our goal is to create a model that can be used under changing climate conditions. As described by Arora (2002) the simulation of vegetation as a dynamic component of the soil–vegetation–atmosphere continuum in hydrological models is crucial when studying climate change and transient climate scenarios. Therefore we chose to make the model as physically based as possible. In order to use a SPAC model on a timescale of 1000 years, an upscaling method was developed that enables us to make long model runs with a daily time step, while still taking into account the non-linearities in the reaction of vegetation in terms of evapotranspiration and carbon assimilation to soil moisture content and (diurnal) variation of atmospheric variables (radiation, temperature and vapor pressure deficit).

The model of Daly et al. (2004) has been used as starting point. This model simulates the soil–plant–atmosphere continuum and is for the main part physically based. In order to use this model for vegetation growth and competition in temperate climates the model was expanded with (i) light and water competition between vegetation types, (ii) oxygen limitation due to high soil moisture contents, (iii) growth and respiration of vegetation and (iv) climatic forcing by a stochastic weather generator. Furthermore, a temporal upscaling method was applied to make the vegetation model suitable for daily time steps and long time series.

In this first article we describe the adapted vegetation model including one-dimensional water and light competition. To test the model, simulation results of evapotranspiration and carbon dioxide fluxes are compared to eddy covariance measurements. A comparison of fluxes is made based on a daily and a yearly timescale. Using this model the influence of groundwater on the vegetation dynamics and soil moisture content on different time scales as well as the influence of soil texture is determined. The results show the importance of studying vegetation and hydrology including groundwater as an integrated system.

The resulting vegetation model is used as a basis for a spatio-temporal vegetation model coupled to a three-dimensional hydrological model. The second article (Brolsma et al., 2010) describes the coupling to a dynamic three-dimensional hydrological model. Using that model we describe the influence of spatial groundwater dynamics on vegetation and vice versa. The coupled vegetation–hydrological model will in future research be used to analyze transient climate scenarios.

2. Model description

The model described in this first paper is a point model, although it can be used as a component in a spatially distributed model, as will be done in the second paper. Although this is a point model, we chose for a spatial extent of 10 m × 10 m which corresponds to the size of a mature tree. First we describe the soil water balance and the atmospheric forcing. Then we describe the vegetation growth model including carbon assimilation, transpiration, interception, respiration and competition for light and water, as well as the upscaling of these processes. Finally, actual vegetation growth, including allocation, allometry, phenology and mortality of vegetation is described.

2.1. Soil water balance

The soil moisture and root water uptake models use a single layer to represent the root zone, with homogeneous soil moisture content. As recently shown by Teuling and Troch (2005) this effectively mimics differential water uptake throughout the root zone throughout the year. The soil moisture model runs on a daily time step. The soil water balance is described by:

$$\frac{d\theta}{dt}Z_r = I - ET - EV + Q_v, \tag{1}$$

where θ is soil moisture content, t [s] is time, Z_r [m] root zone depth, I [m s^{-1}] is infiltration, ET [m s^{-1}] is plant evapotranspiration, EV [m s^{-1}] is soil evaporation and Q_v [m s^{-1}] is the vertical exchange flux with the saturated zone. This flux is calculated using:

$$Q_v = K_\theta \frac{(-dh_{gw} - (\psi_s/g\rho_w))}{dh_{gw}}, \tag{2}$$

where dh_{gw} [m] is the distance of the groundwater to the center of the rootzone, g [m s^{-2}] is the gravitational acceleration, ρ_w [kg m^{-3}] is the water density, K_θ [m s^{-1}] is the unsaturated soil water conductivity and ψ_s [Pa] is the soil matric potential. K_θ and ψ_s are calculated using Mualem–Van Genuchten relationships (van Genuchten, 1980). Note that the upward flux is positive and the downward flux is negative. With regard to Q_v we note that we limit this flux within one integration time step to the difference between $\theta - \theta_{eq}$, where θ_{eq} is the soil moisture content based on the situation where soil moisture content is in equilibrium with the groundwater level (Brolsma and Bierkens, 2007):

$$\theta_{eq} = \frac{\theta_s - \theta_r}{1 + [(\alpha(dh_{gw}/\rho_w g))^n]^m} + \theta_r, \tag{3}$$

in which θ_s and θ_r are the saturated and residual soil moisture content and α, n and m are van Genuchten parameters.

Infiltration (I) is equal to the minimum value of net precipitation, P_{net} [m s^{-1}] and K_θ. When P_{net} exceeds K_θ this is considered as runoff and remove from the cell. The calculation of P_{net} will be described further on. Soil evaporation is assumed to only occur at near saturated conditions ($\theta > \theta_{sat} - 0.01$). When this occurs EV is assumed to be at a potential evaporation rate calculated using the Penman–Monteith equation (Monteith, 1965) for open water conditions.

2.2. Atmospheric forcing

The atmospheric parameters that are used in the vegetation model are: minimum and maximum temperature (T_{min}, T_{max}) [°C], precipitation (P) [m day^{-1} or m 0.5 h^{-1}], shortwave radiation (Rad_s) [W], longwave radiation (Rad_l) [W] and vapor pressure deficit (D). The vegetation model runs on a half-hourly time step. If the above listed variables are available on a half-hourly resolution, these data are used directly. In case these are not available at a half-hourly time step, or if vapor pressure deficit or longwave radiation are not known the following assumptions have been made to obtain half-hourly values.

In these cases, the air temperature during the day is approximated by:

$$T_a = \frac{T_{min} + T_{max}}{2} + \frac{T_{min} - T_{max}}{2} cos\left[(t_d - t_s)2\pi\right], \tag{4}$$

where t_s [day] is a the time lag between the time that T_{max} is reached and noon.

The vapor pressure deficit is based on the difference between saturated vapor pressure at T_{min} and at T_a according to equations summarized in Allen et al. (1998).

The influence of cloud cover on both long wave radiation, Rad_l [W m^{-2}] and shortwave radiation, Rad_s [W m^{-2}] is estimated using the following two empirical equations by Shuttleworth (1993):

$$Rad_s = \left(a_s + b_s \frac{n}{N}\right) Rad_0, \tag{5}$$

where Rad_0 [W m^{-2}] is shortwave radiation at the top of the atmosphere, n [h] is the actual number of sunshine hours per day, N [h] is the maximum sunshine hours per day, a_s [−] is the fraction of Rad_0 on overcast days and $b_s + a_s$ is the fraction of Rad_0 on clear sky days. The net incoming longwave radiation is given by:

$$Rad_l = \sigma T_a^4 (a_e + b_e\sqrt{e_a}) \left(a_c + b_c \frac{n}{N}\right), \tag{6}$$

where σ is the Stefan Boltzmann constant, T_a [K] is the atmospheric temperature and e_a [Pa] is the vapor pressure. a_e [k Pa$^{-0.5}$], b_e, a_c and b_c are empirical constants.

Short wave radiation over the day is then approximated similarly as in Daly et al. (2004):

$$Rad_d = \frac{4Rad_s}{\delta^2}[-t_d^2 + (\delta + 2t_0)t_d - t_0(t_0 + \delta)], \tag{7}$$

where Rad_s [W] is maximum radiation during the day, t_d [day] is time of day, t_0 [day] is time of sunrise and δ [day] is the day length.

The long simulation runs (1000 years) are performed on a daily basis. Minimum and maximum temperature (T_{min}, T_{max}), precipitation (P) and mean global radiation (Rad_0) are generated by a stochastic weather generator (Richardson, 1981). Added to this generator is a reduction function for radiation to account for the effect of cloud cover. Cloud cover is based on a 50 years time series of measurements of fraction of sunshine by the Royal Netherlands Meteorological Organization (KNMI). Cloud cover data have been divided into bins, based on month number, difference between T_{min} and T_{max} and P. Based on the generated temperature difference and P, a sunshine fraction is drawn randomly from the corresponding bin. Vapor pressure deficit (D) is estimated from equations summarized in Allen et al. (1998) based on T_{min} and T_{max}.

2.3. Vegetation growth

To simulate transpiration and assimilation we used the model described in Daly et al. (2004). Here we describe the most important processes and assumptions, as well as the additions and modifications to this model. To allow for competition for light and water, at every location multiple species can grow. In this study we concentrate on a situation with two tree species, which means that understory is not simulated in this study.

The model is based on the single big leaf approach, thus canopy shading and within canopy variation of ambient variables are ignored. Although we are aware of the fact that this can influence both transpiration and growth significantly (e.g. Friend, 2001), to limit calculation times, we did not use a double layer model. Furthermore it is assumed that the plant system acts as a series of steady states, i.e. equilibrium between soil water flux, water flux through the plant and transpiration is reached instantaneously and no storage in the plant is taken into account. The model is sequential in the sense that first transpiration is calculated based on the soil–root–plant conductance and the stomatal conductance. Then the carbon assimilation rate is calculated based on biochemical processes, with the stomatal conductance as a limiting condition.

Transpiration, carbon assimilation, respiration and light interception are calculated on a half-hourly time interval. Rainfall interception can be calculated both on a half-hourly and on a daily time step. All other processes are calculated on a daily time interval. When the model is run for long simulation runs (longer then 1 year) the model is run on a daily time step. In this case fluxes of transpiration, carbon assimilation and light interception are summed to daily values in an upscaling procedure explained hereafter.

2.3.1. Transpiration

The transpiration module is based on Daly et al. (2004) with one modification to account for oxygen stress due to high soil moisture conditions. Transpiration (ET_{srp}) [m day^{-1}] based on the soil–root–plant conductance and water potential in the soil and the leaf per unit ground area [m s^{-1}] can be described by:

$$ET_{srp} = g_{srp}(\psi_s - \psi_l), \tag{8}$$

where g_{srp} [m Pa^{-1} s^{-1}] is soil–root–plant conductance per unit ground area, ψ_s [Pa] soil water potential and ψ_l [Pa] is the leaf water potential. g_{srp} is described by:

$$g_{srp} = \frac{g_{sr} g_p LAI}{g_{sr} + g_p LAI}, \tag{9}$$

where g_p [m Pa^{-1} s^{-1}] is the plant conductance per unit leaf area, g_{sr} [m Pa^{-1} s^{-1}] soil–root conductance per unit ground area and LAI is the leaf area index. g_{sr} is calculated using a simplified cylindrical root model that links the distance traveled by water to reach the root to the root zone depth, Z_r [m], and the root area index RAI using the approach of Katul et al. (2003):

$$g_{sr} = \frac{K_\theta \sqrt{RAI}}{\pi g \rho_w Z_r} f_{ox}(\theta), \tag{10}$$

where K_θ [m Pa^{-1} s^{-1}] is unsaturated soil water conductivity and $f_{ox}(\theta)$ is a reduction function for wet conditions causing oxygen stress in the rootzone. The last function is added to the function of Katul et al. (2003) and model of Daly et al. (2004) to be able to study the effect of high groundwater levels and water stagnation on vegetation. To account for additional root growth as a consequence of dry soil conditions, the RAI is dependent on soil moisture:

$$RAI = RAI \cdot s^{-a}, \tag{11}$$

where a is a parameter that varies from species to species and $s = (\theta - \theta_r)/(\theta_s - \theta_r)$ is soil saturation. The plant conductance depends on leaf water potential ψ_l, because cavitation occurs as a consequence of low water potential in the xylem vessels:

$$g_p = g_{p,max} e\left[-\left(-\frac{\psi_l}{d}\right)^c\right], \tag{12}$$

where $g_{p,max}$ [m Pa^{-1} s^{-1}] is maximum plant conductance (per unit leaf area), c and d [Pa] are parameters to scale ψ_l.

In wet soil moisture conditions, root water uptake can be limited due to a shortage of oxygen in the rootzone. To account for this effect the reduction function f_{ox} is included. This function is based on Feddes et al. (1978) and Brolsma and Bierkens (2007):

$$f_{ox} = \begin{cases} 1 & \text{if } \theta < \theta_{ox,1} \\ \dfrac{\theta_{ox,0} - \theta}{\theta_{ox,0} - \theta_{ox,1}} & \text{if } \theta_{ox,1} < \theta < \theta_{ox,0} \\ 0 & \text{if } \theta > \theta_{ox,0} \end{cases}, \tag{13}$$

where $\theta_{ox,1}$ is the soil moisture content at which root water uptake declines and $\theta_{ox,0}$ is the soil moisture content at which the water uptake stops.

Transpiration ET_{pm} [m s^{-1}] of plants based on atmospheric demand is determined using the Penman–Monteith equation (Monteith, 1965):

$$ET_{pm} = \frac{(\lambda_w \gamma_w g_{ba} \rho_a D + \Delta AR)}{\rho_w \lambda_w [\gamma_w ((g_{ba}/g_s LAI) + 1) + \Delta]}, \tag{14}$$

where λ_w [J kg^{-1}] is the latent heat of water vaporization, γ_w [Pa K^{-1}] the psychrometer constant, g_{ba} [m s^{-1}] the series of conductances of the boundary layer and the atmosphere (per unit

ground area), ρ_a [kg m^{-3}] the air density, D the atmospheric water vapor deficit, Δ [Pa K^{-1}] the slope of the saturated water vapor pressure to temperature relationship, AR [J m^{-2} s^{-1}] the absorbed long- and shortwave radiation and g_s [m s^{-1}] is the stomatal conductance (per unit leaf area). Since g_{ba} is a series of conductances, it can be calculated using $1/g_{ba} = LAI/g_b + 1/g_a$, where g_b [m s^{-1}] is the conductance to the boundary layer (per unit leaf area) and g_a [m s^{-1}] the conductance to the atmosphere (per unit ground area).

The stomatal conductance depends on radiation, air temperature, leaf water potential and CO_2 concentration. The dependence is calculated using the formulation of Jarvis (1976) which is based on applying reduction functions for the environmental variables reducing a maximum stomatal conductance $g_{s,max}$ [m s^{-1}]:

$$g_s = g_{s,max} f_{Rad}(Rad) f_D(D) f_{T_a}(T_a) f_{\psi_l}(\psi_l) f_{CO_2}(CO_2), \tag{15}$$

where $f_{Rad}(Rad)$, $f_D(D)$, $f_{Ta}(T_a)$, $f_{\psi_l}(\psi_l)$ and $f_{CO_2}(CO_2)$ are respectively reduction functions for radiation, vapor pressure deficit, air temperature, leaf water potential and CO_2 concentration in the atmosphere. Daly et al. (2004) shows that the method of Jarvis (1976) leads to similar results as the approach of Leuning (1990).

Reduction of the stomatal conductance as a consequence of vapor pressure deficit is approximated using:

$$f_D(D) = \frac{1}{1 + (D/D_x)}, \tag{16}$$

where D_x is an empirically determined constant (Lohammer in Leuning, 1995). Air temperature influences g_s both at low and high temperatures:

$$f_{T_a}(T_a) = 1 - k_2(T_a - T_{opt})^2, \tag{17}$$

in which k_2 [K^{-2}] is a sensitivity parameter, T_{opt} [K] is the temperature where g_s is at maximum and T_a [K] is air temperature.

The effect of increasing radiation can be expressed as an exponential function such that stomatal conductance increases at high radiation values:

$$f_{Rad}(Rad) = 1 - exp(-k_1 Rad), \tag{18}$$

where k_1 is a sensitivity parameter (Jones 1992 in Daly et al. (2004)). Finally g_s is directly influenced by leaf water potential, where reduction occurs at low leaf water potentials:

$$f_{\psi_l}(\psi_l) = \begin{cases} 0 & \text{if } \psi_l > \psi_{l_0} \\ \dfrac{\psi_l - \psi_{l_0}}{\psi_{l_1} - \psi_{l_0}} & \text{if } \psi_{l_0} < \psi_l < \psi_{l_1} \\ 1 & \text{if } \psi_l < \psi_{l_1} \end{cases}, \tag{19}$$

where ψ_{l_1} [Pa] is the threshold potential at which the root-to-leaf hydraulic conductance begins to decline, ψ_{l_0} [Pa] threshold potential at which the root-to-leaf hydraulic conductance becomes negligible.

Assuming steady states and no storage, ET_{srp} equals ET_{pm}. Then ET, ψ_l and g_s are solved numerically from Eqs. (8), (14) and (15).

2.3.2. Carbon assimilation

Also for the carbon assimilation module the approach of Daly et al. (2004) is followed. Carbon assimilation is determined by the equilibrium between the assimilation based on stomatal CO_2 conductance, $A_{n,g_{sba}}$ [mol m^{-2} s^{-1}], and the assimilation based on the carboxylation capacity of the leaf, $A_{n,bio}$ [mol m^{-2} s^{-1}]. Both are calculated per unit leaf area. The first is described by:

$$A_{n,g_{sba}} = g_{sba,CO_2}(C_a - C_i), \tag{20}$$

where g_{sba,CO_2} [mol m^{-2} s^{-1}] is the series of stomatal, leaf boundary layer and aerodynamic conductances for CO_2, C_a [mol mol^{-1}] is carbon concentration at the leaf surface and C_i [mol mol^{-1}] intercellular carbon concentration. It is assumed that the leaf boundary layer and atmospheric conductance are constant. The conductances for CO_2 are related to the conductance for H_2O by $g_{s,CO_2} = g_s/1.6$ [mol m^{-2} s^{-1}] (per unit leaf area), $g_{b,CO_2} = g_b/1.37$ [mol m^{-2} s^{-1}] (per unit leaf area) and $g_{a,CO_2} = g_a$ [mol m^{-2} s^{-1}] (per unit ground area).

The second is modeled according to the model of Farquhar et al. (1980) and extensions summarized in Leuning (1995):

$$A_{n,bio} = A_{n,\psi_l} min(A_{n,c}, A_{n,q}), \tag{21}$$

where A_{n,ψ_l} is a reduction function for carbon assimilation due to low leaf water potential (ψ_l) and $A_{n,c}$ [mol m^{-2} s^{-1}] and $A_{n,q}$ [mol m^{-2} s^{-1}] are the rubisco limited and the light limited carbon assimilation rate respectively. The reduction of carbon assimilation due to low ψ_l is modeled by:

$$A_{n,\psi_l} = \begin{cases} 0 & \text{if } \psi_l < \psi_{l,A_{n,0}} \\ \dfrac{\psi_l - \psi_{l,A_{n,0}}}{\psi_{l,A_{n,1}} - \psi_{l,A_{n,0}}} & \text{if } \psi_{l,A_{n,0}} < \psi_l < \psi_{l,A_{n,1}} \\ 1 & \text{if } \psi_l > \psi_{l,A_{n,1}} \end{cases}, \tag{22}$$

in which $\psi_{A_{n,1}}$ [Pa] is the threshold potential at which assimilation reduction caused by chemical action begins to decline and $\psi_{A_{n,0}}$ [Pa] is the threshold potential at which assimilation reduction caused by chemical action becomes negligible.

For light limited conditions biochemical driven carbon assimilation per unit leaf area is calculated using:

$$A_{n,q} = \frac{J}{4} \frac{C_i - \Gamma^*}{C_i + 2\Gamma^*}, \tag{23}$$

where J [mol photons s^{-1} m^{-2}] is the incident electron flux resulting from absorbed photosynthetically active radiation (APAR) and Γ^* [mol C mol^{-1} air] is the CO_2 compensation point. The CO_2 compensation point depends on temperature as:

$$\Gamma^* = \gamma_0 \left[1 + \gamma_1(T_l - T_0) + \gamma_2(T_l - T_0)^2\right], \tag{24}$$

where γ_0, γ_1 and γ_2 are empirical constants, T_0 [K] is the reference temperature and T_l [K] is the leaf temperature.

In rubisco limited conditions carbon assimilation is modeled by:

$$A_{n,c} = V_{c,max} \frac{C_i - \Gamma^*}{C_i + K_c\left(1 + o_i/K_o\right)}, \tag{25}$$

where $V_{c,max}$ [mol m^{-2} leaf s^{-1}] is maximum carboxylation capacity, K_c, K_o [mol m^{-2}] are Michaelis–Menten constants for CO_2 and O_2 respectively and o_i [mol m^{-2}] is atmospheric oxygen concentration.

The electron flux depends on:

$$k_1 J^2 - (k_2 Q + J_{max})J + k_2 Q J_{max} = 0, \tag{26}$$

where Q [mol photons m^{-2} s^{-1}] is the absorbed photosynthetically active radiation (APAR), k_1 determines the shape of the non-rectangular hyperbola, k_2 [mol electrons mol^{-1} photons] is the quantum yield of whole-chain electron transport and J_{max} [mol photons m^{-2} s^{-1}] is the potential rate of whole-chain electron transport. The latter is calculated using:

$$J_{max} = J_{max,0} \frac{exp[(H_{vJ}/RT_0)(1 - (T_0/T_l))]}{1 + exp[(S_v T_l - H_{dJ})/(RT_l)]}, \tag{27}$$

where $J_{max,0}$ [mol m^{-2} s^{-1}] is the maximum electron transport rate at T_0, T_0 is 293.2 K, H_{vJ} [J mol^{-1}] is the energy of activation, S_v [J mol^{-1} K^{-1}] is an entropy term and H_{dJ} [J mol^{-1}] is the energy of deactivation.

The Michaelis–Menten coefficients [mol mol^{-1}] are given by:

$$K_x = K_{x0} exp\left[\frac{H_x}{RT_0}\left(1 - \frac{T_0}{T_l}\right)\right], \tag{28}$$

where x stands for c and o, K_{x0} [mol mol^{-1}] is the Michaelis–Menten constant at T_0, R [J K^{-1} mol^{-1}] is the gas constant and H_x [mol m^{-2} s^{-1}] is the activation energy. The maximum carboxylation capacity is given by:

$$V_{c,max} = V_{c,max0} \frac{exp[(H_{vV}/RT_0)(1-(T_0/T_l))]}{1+exp[(S_v T_l - H_{dV})/(RT_l)]}, \quad (29)$$

where $V_{c,max0}$ [mol m^{-2} s^{-1}] is the value of $V_{c,max}$ at T_0, H_{vV} is the energy of activation, S_v [J mol^{-1} K^{-1}] is an entropy term and H_{dV} [J mol^{-1}] is the deactivation energy.

To evaluate the biochemical parameters J_{max}, K_x and $V_{c,max}$ (Eq. (27)–(29)) we need the leaf temperature which is calculated from the closure of the leaf energy balance as:

$$T_l = T_a + \frac{AR - \rho_w \lambda_w ET}{c_p \rho g_{ba}}, \quad (30)$$

where c_p is the specific heat of air [J kg^{-1} K^{-1}].

If g_s, ET and ψ_l are calculated T_l can be calculated from Eq. (30) after which one can calculate Γ^*, J, K_x, and $V_{c,max}$ from Eqs. (24), (26), (28) and (29). A_{n,ψ_l} can be calculated from Eq. (22). Finally we can solve for C_i by equating Eq. (20) to Eq. (21). Assuming equilibrium between atmospheric supply of carbon and biochemical assimilation: $A_{n,bio} = A_{n,g_{sba}}$.

2.3.3. Respiration

To determine the carbon gain and therefore growth of vegetation, also the loss of carbon due to respiration has to be estimated. Total vegetation respiration consists of leaf respiration, above ground wood respiration, fine and coarse root respiration and growth respiration.

Respiration of leaves, stem sapwood, root sapwood, and fine root tissue are modeled according to Sitch et al. (2003); an approach based on Ryan (1991) and Sprugel et al. (1995). In this approach respiration is based on the nitrogen content of different tissues. This nitrogen content is representative of living tissue that respires. Therefore a single nitrogen-based respiration coefficient can be used but differentiation is required for the nitrogen content of the different tissues.

For sapwood tissue respiration a distinction is made for above ground respiration, R_{sws} [mol m^{-2} s^{-1}], and below ground tissue respiration ,R_{swr} [mol m^{-2} s^{-1}], for it is temperature dependent. It is given by:

$$R_{sws} = f_{above} \cdot B_{mol} \cdot f_{sw} \frac{r}{cn_w} f(\overline{T_{day}}), \quad (31)$$

$$R_{swr} = (1 - f_{above}) \cdot B_{mol} \cdot f_{sw} \frac{r}{cn_w} f(\overline{T_{year}}), \quad (32)$$

where r [g C g N^{-1} day^{-1}] is the respiration coefficient, B_{mol} [mol C m^{-2}] is the total species biomass, f_{sw} is the fraction of sapwood, cn_w is the C:N ratio of woody tissue, $f(\bar{T})$ accounts for the dependency of respiration to temperature and f_{above} is the fraction of above ground woody biomass.

Leaf respiration R_l [mol m^{-2} s^{-1}] and fine root respiration R_{fr} [mol m^{-2} s^{-1}] are respectively modeled as:

$$R_l = \frac{LAI}{SLA \cdot C_{mass}} \frac{r}{cn_l} f(\overline{T_{day}}), \quad (33)$$

$$R_{fr} = \frac{RAI}{SRA \cdot C_{mass}} \frac{r}{cn_{fr}} f(\overline{T_{year}}), \quad (34)$$

where C_{mass} [g mol^{-1}] is the mol mass of carbon, cn_l and cn_{fr} are respectively the C:N ratio of leaf and fine root tissue, SRA and SLA are respectively the specific root and leaf area [m^2 kg^{-1} leaf]. The temperature dependencies of the respiration of the above and below ground tissue are calculated using a modified Arrhenius equation:

$$f(T) = exp\left[308.56\left(\frac{1}{56.02} - \frac{1}{T+46.02}\right)\right], \quad (35)$$

where T [°C] is the temperature.

The total respiration R [mol m^{-2} s^{-1}] is the summation of the respiration of all compartments of the tree: $R = R_{sws} + R_{swr} + R_{fr} + R_l$. Net carbon assimilation is than defined as $A_{n,net} = An\_R$. Following Ryan (1991) growth respiration is assumed to be a fixed fraction of the net carbon assimilation: $R_{growth} = A_{n,net} \times 0.3$ and therefore the assimilate that is available for growth is: $A_{n,growth} = A_{n,net} \times (1 - 0.3)$.

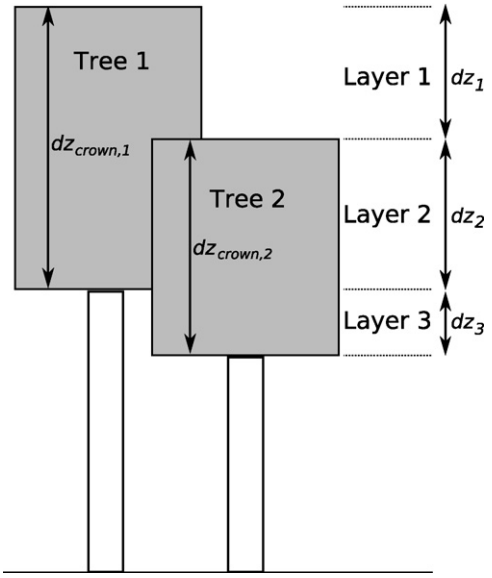

Fig. 1. Scheme used for radiation absorption by trees. In the model concept the trees do not stand next to each other but the LAI is homogeneously distributed over the cell area, thus LAI does fully overlap horizontally.

2.3.4. Light and water interception

Light absorption is calculated for each species present in a cell. A random/homogeneous distribution of the leaves in space between the top and the base of the crown is assumed, where the base of the crown is located at the middle of the height of the tree. The calculation of radiation absorption is explained based on a case of two trees with overlapping crowns (Fig. 1), but it can easily be expanded to cases with more trees. To calculate the absorbed radiation, first the absorption per layer AR_L [W m^{-2}], where L denotes layer number, is calculated based on the total LAI per layer:

$$AR_L = Rad(1-\alpha)\prod_{l=1}^{L}(1 - exp^{-kLAI_l}), \quad (36)$$

where α is the albedo and k is the light extinction coefficient and LAI_l is the total LAI of layer l which in the case of two species is:

$$LAI_l = \sum_{i=1}^{2} \frac{LAI_{l,i} \cdot dz_l}{dz_{crown,i}}, \quad (37)$$

where dz_l [m] is the vertical thickness of the layer ,$LAI_{l,i}$ is the leaf area index of tree i in layer l and $dz_{crown,i}$ [m] is the length of the crown of tree i.

Absorbed radiation per tree can now be calculated as the weighted sum of the absorbed radiation per layer. For every tree

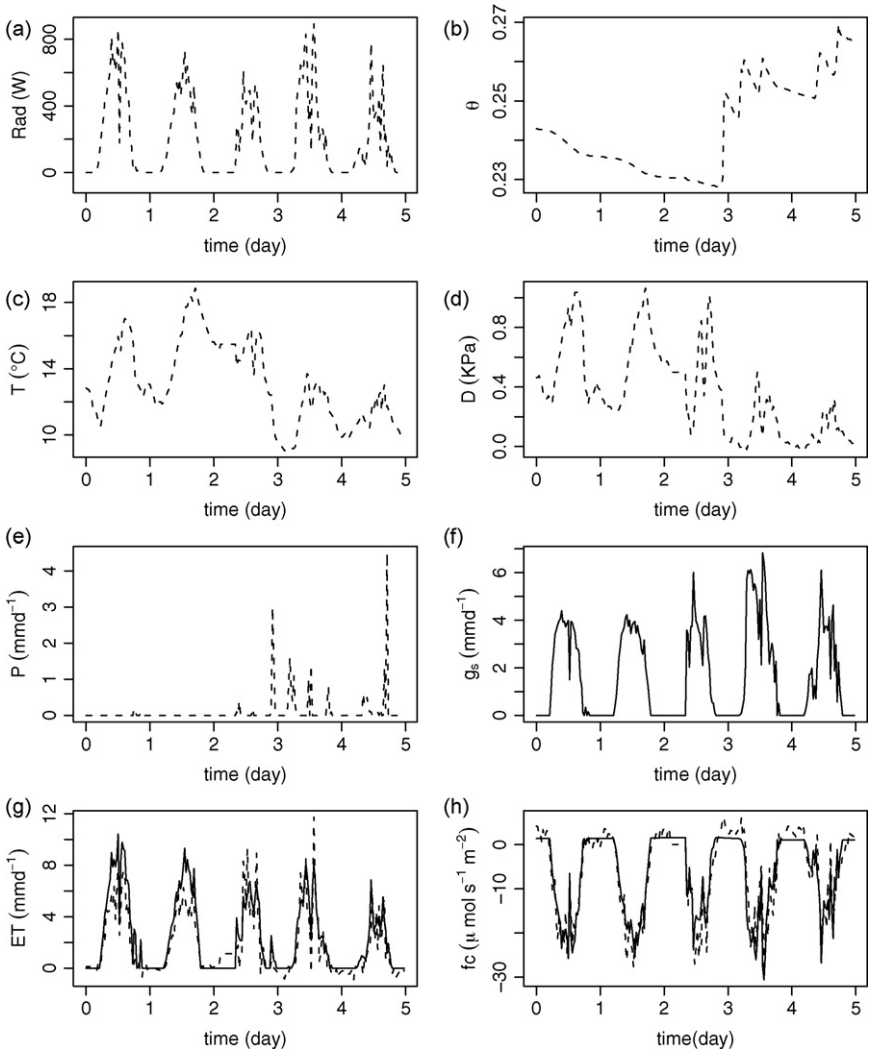

Fig. 2. Comparison of measured and modeled fluxes and stomatal conductance for a 5-day period (days 181–185, 2004) in Hainich forest. Influence of environmental variables: (a) incoming shortwave radiation, (b) soil moisture content θ of root zone, (c) air temperature, (d) water vapor deficit and (e) precipitation on (f) modeled stomatal conductance and (g) evapotranspiration and (h) carbon flux. Dashed lines, measured values; solid lines, model results.

in the cell the absorbed radiation is:

$$AR_i = \sum_{l=1}^{L} \frac{LAI_{l,i}}{LAI_l} AR_l. \tag{38}$$

Precipitation interception is calculated based on the total *LAI* of the canopy and than linearly divided between the individual *LAI* of the tree species that are present. We make the assumption that precipitation falls at a constant rate throughout the given time interval. Part of the precipitation P that reaches the top of the canopy falls on the soil directly as direct throughfall P_d [mm day^{-1}], while part of the precipitation is intercepted P_{int} [mm day^{-1}] depending on the gap fraction f_{gap}:

$$P_{int} = (1 - f_{gap})P. \tag{39}$$

The gap fraction is estimated using only the transmittance part of Eq. (36):

$$f_{gap} = e^{-kLAI}. \tag{40}$$

When running the model on a daily time step we assume that as long as the interception capacity of the canopy is not exceeded and the open water evaporation for a day is not exceeded all water is intercepted:

$$I = E_I = min\left(E_O, LAI \cdot \frac{I_{cap}}{\Delta t}, P_{int}\right), \tag{41}$$

where I [mm day^{-1}] is interception, E_I [mm day^{-1}] is evaporation of interception, E_O [mm day^{-1}] is open water evaporation that is calculated using the Penman–Monteith equation (Monteith, 1965) applied to open water, Δt [day] is the time step size and I_{cap} [mm] is the maximum interception capacity.

When running the model on a semi-hourly time step, I is not limited to E_O. This means that the intercepted water from the previous time step that has not yet evaporated is still present in the canopy, thus:

$$I_t = min\left(max\left(I_{t-\Delta t} + P_{int} - E_O, 0\right), LAI \cdot \frac{I_{cap}}{\Delta t}\right), \tag{42}$$

where t denotes time and Δt [0.5 h] is the time step size. In both cases precipitation that reaches the ground as throughfall is:

$$P_{net} = P - I. \tag{43}$$

During the time needed for evaporation of the interception, transpiration is neglected.

Table 1
Values of parameters to fill lookup table of Tr and A_n. Min and Max are the minimum and maximum values of the range for which transpiration and assimilation values have been calculated. Nr of steps indicates the number values between the minimum and maximum value have been calculated. Step size is the interval between the subsequent values of the calculated values of the lookup values. var means that an exponential function is used produce variable step sizes for lookup values.

Parameter	Min	Max	Nr of steps	Step size	Unit
LAI	0.1	5	21	var	–
θ	θ_r	θ_{sat}	22	var	–
T_{max}	0	40	8	5	[°C]
T_{min}	$T_{max}-30$	T_{max}	7	5	[°C]
Rad_{max}	0	800	20	var	[W m^{-2}]
n/N (cloud coverage)	0	1	6	0.2	–
δ (day length)	8	16	5	2	[h]

2.4. Temporal upscaling

To perform long simulation runs, the vegetation model that runs on a time scale of half an hour, has to be scaled up. During the day, meteorological parameters such as radiation, temperature and water vapor pressure deficit vary while they influence transpiration (ET) and carbon assimilation (A_n) in a non-linear way. This means that a simple linear upscaling using average values of the input variables leads to biased results. We therefore use the following upscaling procedure. First it is assumed that fluxes during a half hour time interval are constant. An interval of half an hour is chosen, because this corresponds to the eddy-covariance flux measurement integration and report interval. Also, smaller time steps then a half hour would cause a significant increase in computation time, whereas larger time steps would not capture the daily variation. Assuming the daily course in temperature and radiation are as described in Eqs. (7) and (4), on a daily timescale seven variables influence ET and A_n: T_{min}, T_{max}, Rad, δ (day length), n/N (time fraction cloud coverage), θ and LAI. The range in values of each of these variables is discretized in steps (Table 1). Day sums of ET and A_n for all possible combinations of these variables between reasonable bounds are calculated and stored in a lookup table. For LAI and Rad, the step size increases with higher values because the system is most sensitive at lower values. For θ the step size is smaller for both high and low values for the same reason. Because the difference between T_{min} and T_{max} during a day is limited T_{min} is defined relative to T_{max} with a maximum difference of 30 °C. When performing long runs, daily values of T_{min}, T_{max}, Rad, δ, n/N, θ and LAI are generated or calculated and the associated ET and A_n is then directly read from the table. The filling of the table takes quite some time (app. 2 days on a PC), requiring the calculation of ET and A_n at half-hourly time step for $21\times22\times8\times7\times20\times6\times5=1.55\times10^7$ parameter combinations. However once filled, long simulation runs (hundreds of years) using realistic A_n and ET values at a daily time step are possible.

2.5. Growth, allocation, allometry and phenology

To calculate light competition between trees we need to know the height of the trees H [m] and the LAI. We also need to know the LAI to calculate leaf respiration and carbon allocation. Because these parameters vegetation are difficult to calculate based on biomechanical principles, allometric scaling relationships have been used to relate them to biomass per unit area.

The geometry of the trees is based on woody biomass. The woody biomass is divided in above ground biomass B_{above} [kg m^{-2}] and below ground biomass B_{below} [kg m^{-2}]:

$$\begin{aligned} B_{above} &= f_{above}B \\ B_{below} &= (1-f_{above})B \end{aligned}, \tag{44}$$

Table 2
Soil textures used in simulation runs. θ_{sat} saturated soil moisture content; θ_r residual soil moisture content; K_s [m day^{-1}] saturated conductivity; α [m^{-1}] and n van Genuchten parameters (Carsel, 1988).

Soil texture	θ_{sat}	θ_r	K_s [m day^{-1}]	α [m^{-1}]	n
Loamy sand	0.41	0.057	3.50	12.4	2.28
Sandy loam	0.41	0.065	1.06	7.5	1.89
Sandy clay loam	0.39	0.100	0.134	5.9	1.48
Silty clay loam	0.43	0.089	0.0138	10.0	1.23
Loamy clay	0.51	0.102	0.71	1.27	1.38

where B [kg m^{-2}] is the dry biomass of the woody parts of the tree, f_{above} is the above ground fraction of biomass. The value of f_{above} is fixed during growth and the same for all species.

The canopy is simplified by assuming that the canopy is homogeneous between its base and its top, where its base is located halfway the top of the canopy and the ground. It is assumed that 40% of the above ground biomass is located in the stem and 60% in the branches. The number of trees per area [trees ha^{-1}] is calculated using:

$$n_{tree} = a_{nrtree} + b_{nrtree}e^{-c_{nrtree}B_{above}}, \tag{45}$$

where a_{nrtree}, b_{nrtree} and c_{nrtree} are empirical parameters. The function is fitted on data form Jansen et al. (1996). From this it follows that the stem biomass per tree B_{stem}, [kg] is:

$$B_{stem} = \frac{B_{above}10^4}{n_{tree}}, \tag{46}$$

where 10^4 is a factor to convert from m to ha [m^2 ha^{-1}]. When the wood density is known(ρ_{stem} [kg m^{-3}]) the wood volume per tree, V_{stem} [m^3], is:

$$V_{stem} = \frac{B_{stem}}{\rho_{stem}}. \tag{47}$$

The diameter of the stem at breast height (D_{stem}) [m] is given by (e.g. Landsberg, 1986):

$$D_{stem} = \frac{(B_{stem}/a_{md})^{(1.0/b_{md})}}{100}, \tag{48}$$

where a_{md} and b_{md} are allometric scaling factors and 100 is a factor to convert from cm to m.

Assuming a cylindrical form of the stem of a tree, the height of a tree H_{tree} [m] is given by:

$$H_{tree} = \frac{V_{stem}}{(D_{stem}/2)^2\pi}. \tag{49}$$

So through Eqs. (44)–(49) height and number of trees is related to biomass m^{-2}. We assume a fixed relationship between RAI and LAI:

$$RAI = LAI_{max}\cdot RAI_{frac}. \tag{50}$$

The maximum LAI depends on the sapwood area (pipe theory Shinozaki in Friend et al., 1997):

$$LAI_{max} = \eta_f Z_{sw}, \tag{51}$$

where η_f is the sapwood to foliage ratio and Z_{sw} sapwood area at breast height [m^2]:

$$Z_{sw} = \frac{f_{sw}{D_{stem}}^2\pi}{4}, \tag{52}$$

where f_{sw} is the fraction of sapwood to total wood. It depends on an allometric scaling factor:

$$f_{sw} = exp(a_{sw}B_{above}), \tag{53}$$

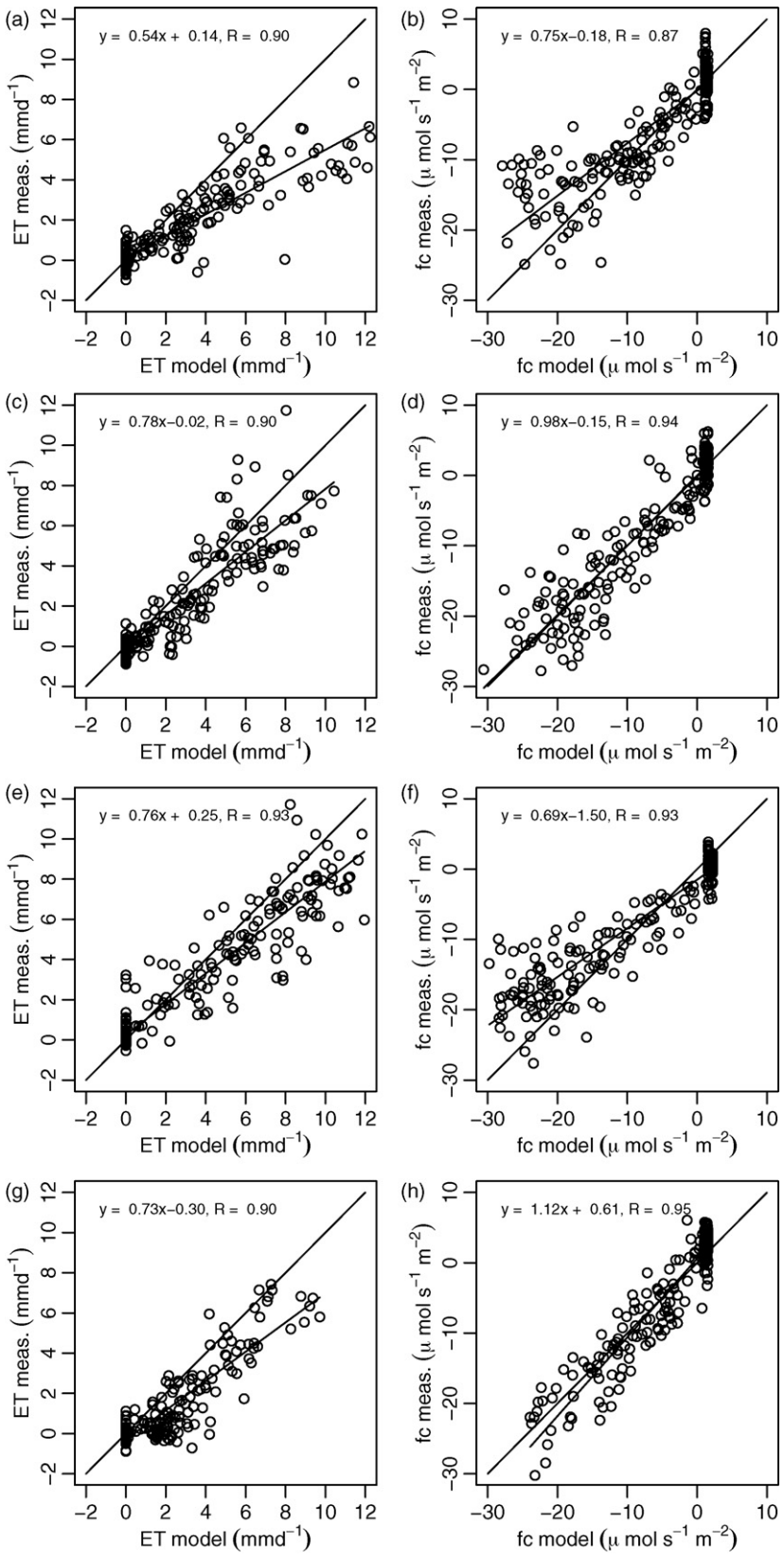

Fig. 3. Modeled versus measured half-hourly flux data of *ET* (left) and CO_2 (right) for four 5-day periods in 2004. Both the 1:1, and the fitted regression line are plotted. Panels (a) and (b), days 150–155; (c) and (d), days 180–185; (e) and (f), days 210–215; (g) and (h), days 240–245. Day 1 is January 1st. Each dot represents one time step of 0.5 h.

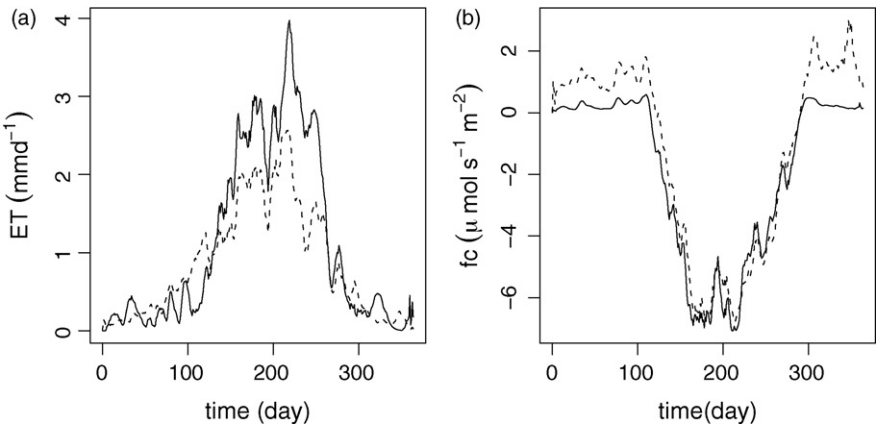

Fig. 4. Daily values of measured and modeled fluxes of *ET* (a) and CO_2 (b) in Hainich Forest in 2004 using a 10 days running means filter. Modeled data are plotted as a solid line and measured data are plotted as a dashed line.

where a_{sw} is a parameter controlling the sapwood area based on the tree biomass. The biomass of the sapwood can then be calculated using:

$$B_{sw} = B_{stem} f_{sw}. \tag{54}$$

Phenology depends on the 10-day maximum temperature sum. When this sum exceeds 100 ° C leaves start to grow at a maximum growth rate that is a fraction of LAI_{max}:

$$LAI_t = LAI_{t-\Delta t} + LAI_g \cdot LAI_{max} \Delta t, \tag{55}$$

where LAI_g [day^{-1}] is the LAI growth rate. The carbon consumed in growth is subtracted from the carbon storage, which can result in a decline in the growth rate when the storage gets depleted. At the end of the growing season, when the 10-day maximum temperature sum becomes lower than 100 °C, leaves start to be shed in a similar way as growth at a fixed rate LAI_d, where the carbon of the leaves is lost.

Carbon allocation is calculated for each species on a daily time step. Each time step carbon assimilate is allocated to a carbon storage compartment [mol]. From the beginning of the growing season, carbon from this storage compartment is used for leaf growth, until LAI_{max}, is reached or until the carbon storage compartment is depleted to 10% of its maximum *S*. When LAI_{max} is reached the carbon assimilate keeps being allocated to the carbon storage compartment until its maximum capacity. When the carbon storage compartment is filled upto maximum, carbon assimilate is used for biomass growth of the woody parts. Biomass growth of the woody biomass occurs at the above mentioned fractions to the stem and the roots. The amount of carbon used for leaf growth depends on the *LAI* and *SLA*:

$$B_{lai} = \frac{LAI}{SLA}, \tag{56}$$

where *SLA* [m^2 kg^{-1} leaf] is the specific leaf area index. The capacity of the carbon storage compartment *S* [kg m^{-2}] is limited to a fixed fraction of the sapwood (Friend et al., 1997):

$$S = f_{store} \times B_{sw}, \tag{57}$$

where f_{store} is the fraction of sapwood that can be used for carbon storage. When the store becomes depleted the tree dies, as it does not have enough storage left to make new leaves the next growing season. Note that the last 10% of the carbon storage can only be used for respiration, not for leaf growth.

2.5.1. Vegetation mortality

As mentioned in the previous paragraph, vegetation dies when the carbon storage becomes depleted. In addition to this assumption a random mortality rate is included to account for death as a result of disease, wind, lightning. Assuming an average tree age of

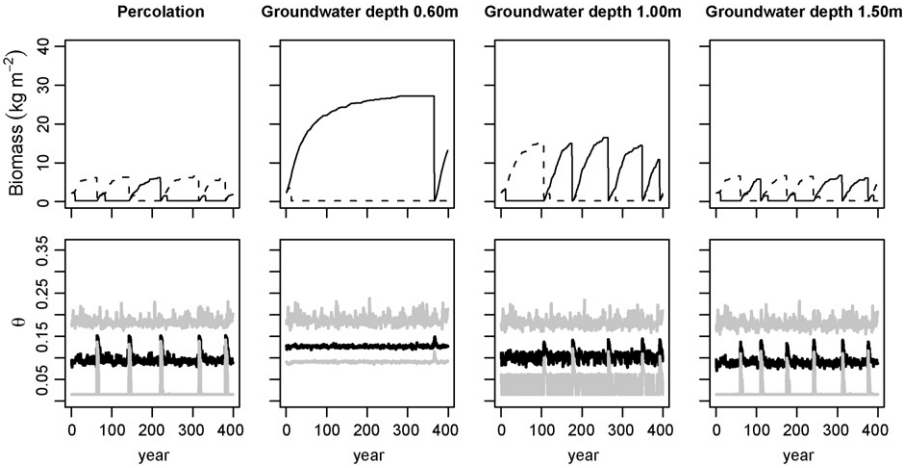

Fig. 5. Development of biomass (top) and soil moisture (bottom) of a wet adapted and a drought adapted vegetation type in a case with percolation only and three different groundwater depths on sandy loam. Top: solid line, wet adapted vegetation; dashed line, dry adapted vegetation. Bottom: black line, yearly average soil moisture content; gray line, yearly minimum and maximum soil moisture content.

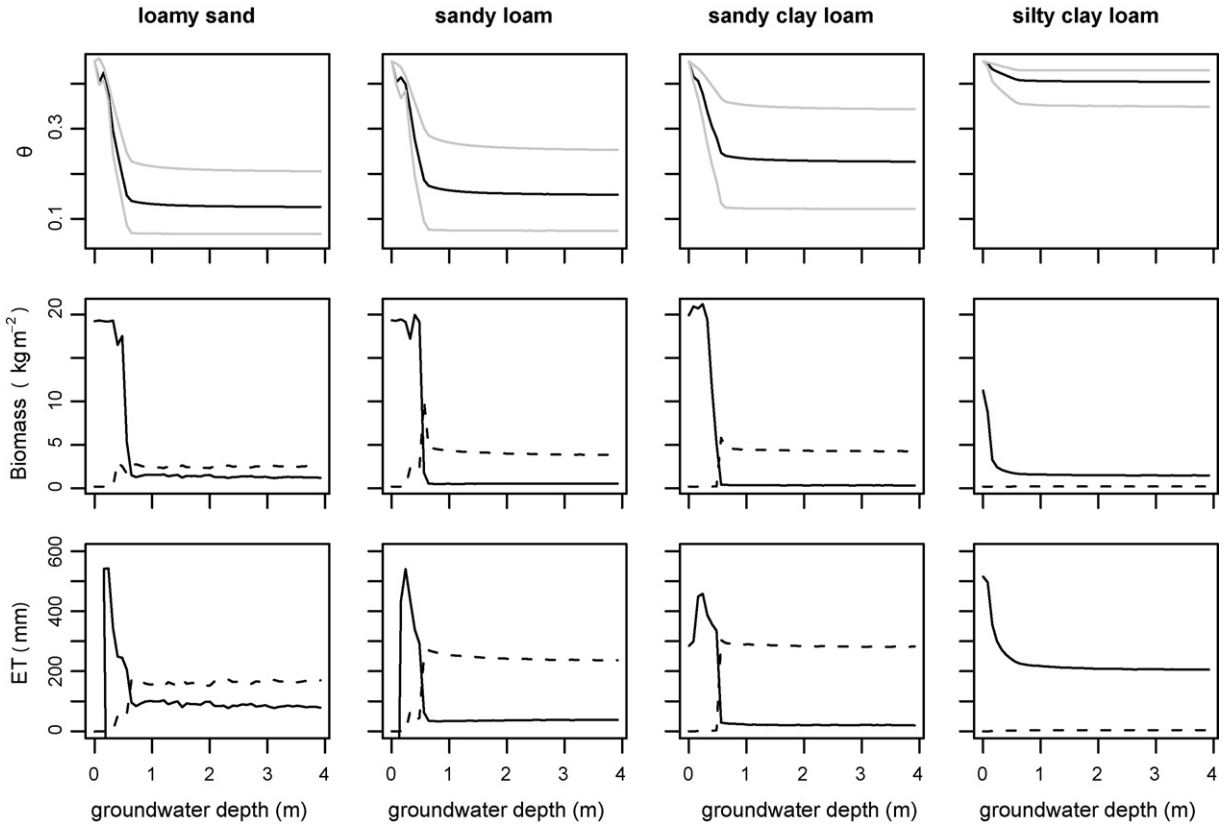

Fig. 6. 500-Year average of biomass, evapotranspiration and yearly minimum, maximum and mean soil moisture content along a groundwater gradient for four soil textures. Biomass and *ET*: solid line, wet adapted vegetation, dashed line, drought adapted vegetation. Soil moisture content: black line, average, gray line, minimum and maximum.

300 years under unstressed circumstances the probability of dying in a given year is 1/300. This is implemented in the model such that when this happens the biomass of both species in a cell is reset to the initial condition.

3. Results

The model has been evaluated on a short timescale by comparing the simulated and measured fluxes of H_2O en CO_2 at 0.5 h time intervals. Using the evaluated model long term simulation runs were performed to investigate the influence of light competition and the influence of groundwater on vegetation dynamics. Parameter values for these runs were taken from literature or in some cases submodules were calibrated against data (Appendix A).

3.1. Comparison with fluxdata

To evaluate the model we compared model simulations with measured evapotranspiration (*ET*) and CO_2 eddy covariance flux data from Hainich forest in Germany (Knohl et al., 2003). This location was chosen because it is a broadleaf forest and it is located in the temperate climate zone. The dataset also contains data of soil moisture content, atmospheric water vapor concentration, temperature and radiation. The model was run with a 0.5 h time step corresponding to the integration and reporting interval of the fluxdata. For this runs the soil texture of Hainich Forest is used which is a loamy clay. Its soil physical parameters (Table 2) are estimated based on a neural network-based ROSETTA database (Schaap et al., 1998). In this analysis the soil water balance is not calculated and therefore the influence of the groundwater is not included. Instead the measured soil moisture content is used.

Fig. 2 shows the main environmental input variables, the resulting stomatal conductance and *ET* and CO_2 fluxes in summer for day 180 until day 185 (day 1 is January first). It can be seen from Fig. 2g and h that the modeled fluxes show a trend that is similar to the measured fluxes. During the day, the *ET* flux is somewhat overestimated by the model. The measured carbon fluxdata show an upward flux during the night, caused by respiration. In the model this flux is underestimated because only autotrophic respiration is included and soil respiration is ignored.

Fig. 3 shows the modeled versus the measured *ET* and CO_2 flux data for four 5-day periods. The correlations of *ET* during the growing season are high ($R = 0.88$–0.93). However *ET* fluxes are overestimated by the model especially in spring and autumn. Correlations between the modeled and measured CO_2 flux are higher ($R = 0.91$–0.94) with no apparent bias.

Table 3
Parameters of the tree species adapted to dry and wet conditions.

Parameter	Description	Wet species	Dry species
ψ_0	Leaf water potential below which g_s becomes 0 [Pa]	−0.45e+06	−4.5e+06
ψ_1	Leaf water potential below which g_s begins to decline [Pa]	−0.005e+06	−0.05e+06
$\psi_{A_n,0}$	Leaf water potential below which assimilation becomes 0 [Pa]	−0.45e+06	−4.5e+06
$\psi_{A_n,1}$	Leaf water potential below which assimilation begins to decline [Pa]	−0.05e+06	−0.5e+06
Ox_0	Soil moisture content above which root water uptake begins to decline	$\theta_{sat} - 0.03$	$\theta_{sat} - 0.10$
Ox_1	Soil moisture content above which root water uptake becomes 0	$\theta_{sat} - 0.01$	$\theta_{sat} - 0.05$

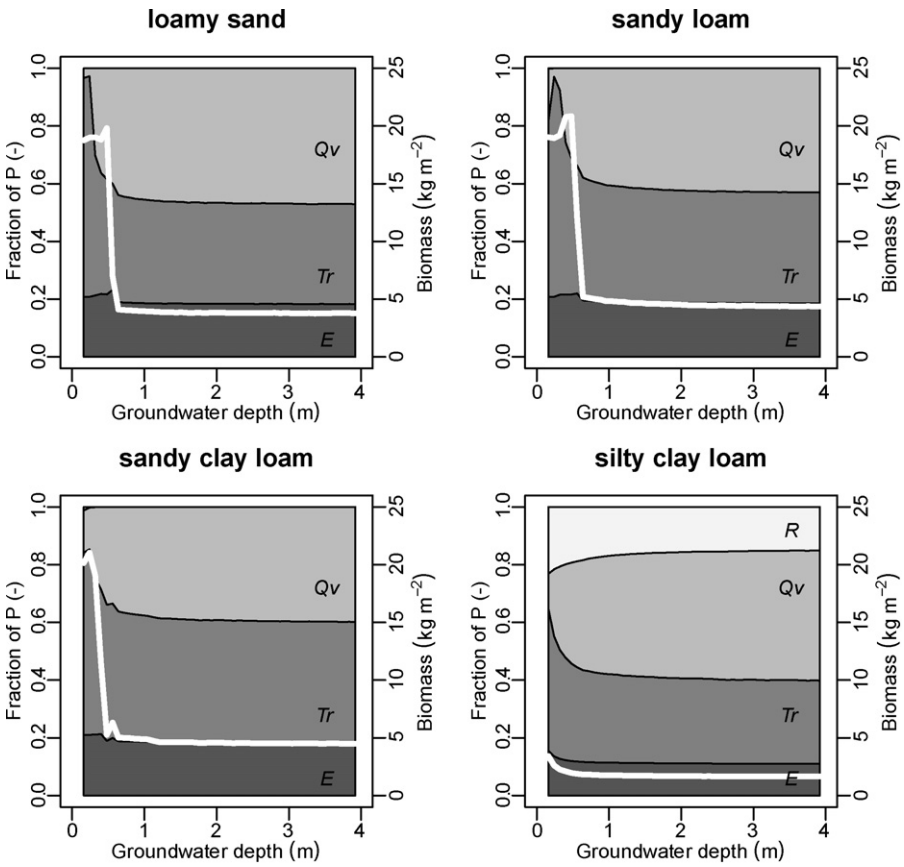

Fig. 7. Influence of groundwater depth on the water balance and biomass for four different soil textures based on 500 years average values. *E*, evaporation; *Tr*, transpiration; *Qv*, vertical exchange flux between unsaturated zone and groundwater; *R*, surface runoff. Fluxes are given as fraction of precipitation (*P*). The white line represents the biomass.

We also compared modeled and measured *ET* and CO_2 on a yearly timescale summing fluxes over a day. Fig. 4 shows the results for 2004. During summer *ET* is overestimated by the model. The net modeled CO_2 flux is underestimated during winter. The latter is largely caused by absence of litter decomposition and soil respiration in the model, which is especially apparent in winter.

The cause for the overestimation of *ET* during summer in the model compared to the measured data is not clear. Causes can be found in one of the many assumptions made in the model. Probable explanations are that the vapor pressure deficit (*D*) as input for the model is overestimated as it is observed above the canopy of the forest, instead of within the canopy. Also the part of the radiation used for transpiration may be over-estimated by neglecting the heat capacity of the canopy.

3.2. Light and water competition and the influence of groundwater

For the long simulation runs of 600 years, climatic forcing by a stochastic weather generator is used, based on Dutch climate conditions, which is characterized by an annual precipitation of 700 mm, a mean summer temperature of 17.7 °C, and a mean winter temperature of 3.4 °C. The long simulation runs have been performed for four different soil textures: loamy sand, sandy loam, sandy clay loam and silty clay loam, of which soil physical parameters are listed in Table 2. For the long simulation runs a spin-up period of 400 years has been used to obtain equilibrium situation in vegetation and hydrological system. All long simulation runs were performed with a combination of two vegetation species; one which is adapted to dry circumstances (e.g. oak) and one that is better adapted to wet circumstances (e.g. alder). Table 3 gives parameters that determine the soil–root-resistance and carbon assimilation reduction due to low leaf water potential.

3.2.1. Influence of groundwater

To illuminate the role of groundwater in vegetation dynamics we performed simulations for a case in which only percolation occurs and three cases with different groundwater levels that result in fluxes between groundwater and soil water. These simulation runs were performed with sandy loam as soil texture. In the case with percolation only, percolation only occurs when field capacity is exceeded. Percolation rate is then equal to K_θ. Fig. 5 shows the development of biomass of the two vegetation types in time. In case of a model in which only percolation occurs, biomasses up till 7 kg m^{-2} are reached. In this case both the wet and the dry species can grow, although the dry species has a slight advantage.

When a fixed groundwater table is included in the model Eq. (2) a capillary flux from the saturated to the unsaturated zone occurs and results are quite different. In the case where the groundwater is directly underneath the rootzone (0.6 m below the surface) the wet adapted species outcompetes the dry adapted species. A maximum biomass of 28 kg m^{-2} is reached and rootzone soil moisture content varies between 0.14 and 0.25. Because of the small distance between the rootzone and the groundwater, capillary rise in summer is high and water stress is therefore low.

If the groundwater level is deeper (at 1.0 m), soil moisture content decreases as well as the lifetime and biomass of vegetation. The decrease in soil moisture content is a direct effect of the deeper

Table 4
Biomass (B), Evaporation (E), Transpiration (Tr), flux between soil and ground water (Qv) and surface runoff (R) for three groundwater levels (Gwd) for four soil textures. Mean yearly precipitation per year is 702 mm. 0 and 1 for B, E and Tr denote respectively the wet adapted and the dry adapted vegetation.

Soil texture	Gwd	B_1	B_2	B	E_1	E_2	E	Tr_1	Tr_2	Tr	Qv	R
Loamy sand	0.2	15.8	0.2	16.0	138	9	146	490	0	490	65	0
	0.6	4.4	1.9	6.3	108	55	163	177	64	241	299	0
	1.5	1.4	2.1	3.5	52	74	125	89	141	230	346	0
Sandy loam	0.2	16.0	0.2	16.2	138	9	147	398	0	398	156	3
	0.6	1.9	8.9	10.9	41	113	154	69	239	309	239	0
	1.5	0.5	4.0	4.5	25	107	132	34	237	271	299	0
Sandy clay loam	0.2	17.2	0.2	17.4	138	9	147	420	0	420	126	17
	0.6	0.5	5.5	6.0	22	117	139	38	284	321	241	0
	1.5	0.4	4.3	4.6	18	111	129	22	273	296	277	0
Silty clay loam	0.2	3.5	0.2	3.7	102	9	112	337	0	337	84	338
	0.6	1.8	0.2	2.0	73	11	84	218	2	219	264	269
	1.5	1.5	0.2	1.7	68	12	79	197	3	200	308	230

groundwater, increasing the downward flux because of the lower water potential and decreasing capillary rise due to the longer distance between the rootzone and the groundwater. The smaller biomass is a result of the lower soil moisture content. This lower soil moisture content causes a lower ψ_s influencing the $\psi_l - \psi_s$ gradient. At the same time the lower soil moisture content causes a lower K_θ which causes a lower soil–root–plant conductance (g_{srp}). This results in smaller g_s, lower ψ_l and therefore less ET. As a final result A_n becomes smaller. Additionally due to less ET the leaf temperature increases and maintenance respiration increases. The decrease in A_n and increase in respiration finally results in a lower biomass.

When random mortality of vegetation due to diseases, wind of lightning is not included, vegetation in the model still dies after a certain period. As the trees grow larger, the margin between assimilation and maintenance respiration becomes smaller. As a period with favorable assimilation and growth conditions is always followed by a period of less favorable conditions where respiration is larger than assimilation, the chance of the storage being depleted increases when vegetation approaches its maximum biomass.

At a low biomass the LAI per volume of sapwood is higher than at a high biomass. Since carbon storage is a fixed fraction of the sapwood, vegetation with a low biomass has a relatively smaller carbon storage. The effect is that vegetation with a lower biomass due to high stress, is more prone to a depleted carbon buffer and thus lives shorter.

When the groundwater is at 1.5 m the yearly minimum soil moisture content approaches the residual moisture content every year and the average yearly soil moisture content drops slightly. Biomasses remain smaller and circumstances for the dry adapted species become more favorable. Because of the high water retention capacity of sandy loam, the wet species is not yet fully outcompeted.

From the model results it becomes clear that besides the soil moisture content, light competition plays an important role. Once a species has established under unfavorable soil moisture conditions, it cannot be outcompeted by another species with a smaller biomass even if the latter is better adjusted to the current soil moisture conditions. In case that one species dies its biomass is reset to a primordial amount. The other species can have a small advantage because it already has a larger biomass. The difference in biomass after death and the suitability of that species to grow at that location determines whether the species that died can outcompete the other vegetation. This causes the alternation of the two species in time.

3.2.2. Longterm influence of groundwater and soil texture

To determine the combined influence of soil texture and groundwater on soil moisture and vegetation growth, we used a gradient in groundwater levels from 30 cm to 400 cm for four different soil textures. This fixed groundwater level influences both percolation and capillary rise.

Fig. 6 shows that soil texture and groundwater depth have a large influence on soil moisture content and biomass. The first thing to note is that silty clay loam leads to completely different results than the soil textures with higher conductivities and lower soil water retention capacities. Silty clay loam remains permanently near saturation, only allowing for growth of the wet species. Even this species, does not attain high biomasses due to oxygen stress, but also due to water stress that mainly results from the low soil water conductivity and high water retention capacity. As to be expected, the decrease in soil moisture conductivity and increase in water retention capacity in the sequence of loamy sand, sandy loam and sandy clay loam, causes higher soil moisture contents. The maximum soil moisture content is largely influenced by precipitation and the groundwater recharge at the and of winter, whereas the minimum soil moisture content is mainly influenced by throughfall and the vegetations capability to transpire water from the dry soil in summer.

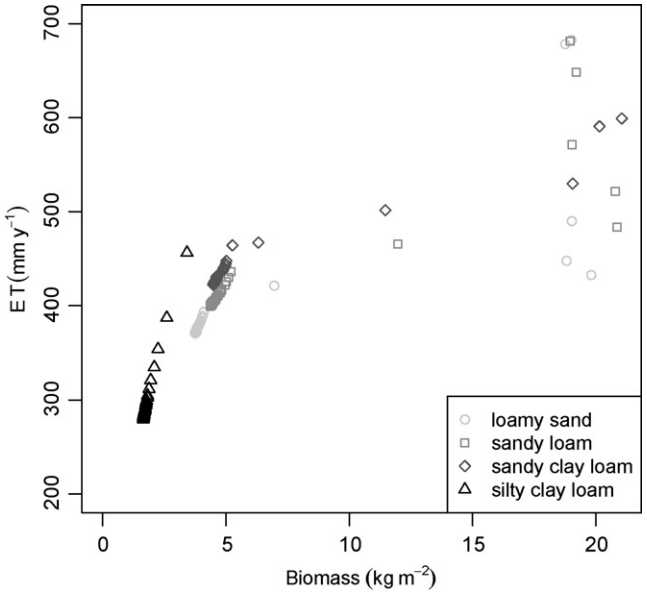

Fig. 8. Dependence of ET on biomass for four soil textures. Biomass and ET are 500 years averages along a gradient of groundwater depths (0.2–4.0 m).

Vegetation growth on loamy sand, sandy loam and sandy clay loam is rather similar for a groundwater depth less than approximately 70 cm. The proximity of groundwater for all soil textures results in a smaller net flux to the groundwater and therefore relatively high soil moisture contents. The wet vegetation attains approximately the same high biomasses on all soil textures.

At approximately 70 cm the biomass of the wet adapted vegetation drops sharply and the dry species prevails. In reality this drop will not be this abrupt, because the rooting depth is more variable. When groundwater becomes deeper, the soil textures with higher water retention capacities and lower conductivities cause the soil moisture content to be higher and the dry vegetation to obtain slightly higher biomasses. At groundwater levels deeper than 70 cm the wet adapted vegetation on loamy sand reaches relatively high biomasses relative to the wetter sandy loam and sandy clay loam. This is caused by the fact that the dry adapted vegetation experiences more water stress in summer, causing less carbon assimilation and therefore lower biomasses and a shorter lifetime. The wet vegetation therefore receives more radiation giving it more opportunities to grow.

3.2.3. Water balance

To get more insight into the interaction between biomass growth and hydrology we constructed Fig. 7 showing the most important water balance components: evaporation (E), transpiration (Tr), vertical soil water flux (Q_v) and runoff (R) as well as the biomass for each soil texture. For reference Table 4 provides the water balance for all cases investigated. It is clear that for most deep open soils as considered here the majority of runoff occurs through groundwater. Surface runoff by rain on saturated soils only occurs for impermeable soils (or shallow aquifers as will be shown in the companion paper).

The absence of understory (apart from the under growing second species) in the vegetation model influences the water balance. Although the model accounts for soil evaporation under near saturated circumstances, both interception evaporation and transpiration are expected to increase the total evapotranspiration if understory of shadow-tolerant species is accounted.

What is obvious from the results is that there is no clear relation between soil texture and the division between evaporation, transpiration, groundwater recharge and runoff, nor does such a relation exist for groundwater depths. Instead, this division between evapotranspired and infiltrated water strongly depends on the biomass as can be seen in Fig. 8. Note that in this figure both biomass and ET are influenced by groundwater depth. Whether caused by a combination of soil texture and groundwater depth that favors one or both species is of no consequence. As long as total biomass is high, a large part of the precipitation will be evapotranspired instead of discharged through groundwater or surface runoff. This clearly shows the importance of a good representation of vegetation growth for hydrology.

4. Conclusions

We have developed a coupled soil moisture–groundwater–vegetation model that is able to simulate the effect of groundwater depth and soil moisture on vegetation growth and vice versa. The model is able to provide estimates of the variation of evapotranspiration (ET) and carbon assimilation (A_n) at hourly, daily and yearly time scales, as well as centennial-scale simulation of forest growth under water and light competition. The results of the 500 years simulation runs clearly demonstrate the importance of light competition in temperate forests: species established under unfavorable soil moisture conditions can almost not be outcompeted by a smaller species that is better adapted to the local soil moisture regime. Only under extremely wet conditions the wet adapted species can outcompete the dry adapted species, or if the difference in biomass between species is very small, i.e. at a very low biomass, a better adapted smaller species can outcompete taller. The influence of groundwater is present for a large range of groundwater depths, by both capillary rise and possible reduction of percolation to the groundwater, while soil texture is important as well, particularly for higher clay contents. 500-Year simulation runs clearly show that groundwater and soil texture have a large impact on biomass development and species composition, i.e. groundwater depth and soil texture determine what species is most successful. In turn species composition and biomass are important predictors for the long term water balance and therefore energy balance of the eco-hydrological system. This study shows that for ecosystems, models for systems with shallow groundwater can greatly be improved by including fluxes from and to the groundwater. The companion paper will show the influence of incorporating groundwater dynamics.

Acknowledgments

This work was sponsored by the Stichting Nationale Computerfaciliteiten (National Computing Facilities Foundation, NCF) for the use of supercomputer facilities, with financial support from the Nederlandse Organisatie voor Wetenschappelijk Onderzoek (Netherlands Organization for Scientific Research, NWO).

Appendix A. Parameters

Tables A.1–A.4.

Table A.1
General parameters.

Variable	Value	Unit	Description	Source
γ_w	0.0	Pa K^{-1}	Psychrometer constant	Daly et al. (2004)
λ_w	2,500,000	J kg^{-1}	Latent heat of water vaporization	Daly et al. (2004)
ρ_{air}	1.2	kg m^{-3}	Air density	Daly et al. (2004)
ρ_w	1000	kg m^{-3}	Water density	–
c_p	1012	J kg^{-1} K^{-1}	Air specific heat at constant pressure	Daly et al. (2004)
G	9.81	m s^{-2}	Gravitational acceleration	–
P	1,01,325	Pa	Air pressure	–
R	8.31	J mol^{-1} K^{-1}	Gas constant	–

Table A.2
Atmospheric parameters (wg = from weather generator).

Variable	Value	Unit	Description	Source
δ	–	h	Day length	Variable
Δ	–	Pa K^{-1}	Slope of the water vapour pressure to temperature	Variable
a_s	0.25	–	Fraction of Rad_0 on overcast days	Allen et al. (1998)
a_c	0.25	–	Empirical constant	Allen et al. (1998)
a_e	0.34	–	Empirical constant	Allen et al. (1998)
b_s	0.5	–	Empirical constant	Allen et al. (1998)
b_c	0.75	–	Empirical constant	Allen et al. (1998)
b_e	−0.14	kPa−0.5	Empirical constant	Allen et al. (1998)
C_a	360	mol mol^{-1}	Carbon concentration of atmosphere	Daly et al. (2004)
D	–	Pa	Vapor pressure	wg
D_x	0.0077	kg kg^{-1}	Water vapor 'max' deficit	Daly et al. (2004)
e_{max}	–	kPa	Saturation vapour pressure at T_{max}	Variable
e_{min}	–	kPa	Saturation vapour pressure at T_{min}	Variable
e_a	–	kPa		Variable
N	–	h	Maximum number hours of sunshine	wg
n	–	h	Actual number of hours of sunshine	wg
P	1,01,325	Pa	Air pressure	Mean at sealevel
Rad_{max}	–	W	Maximum radiation at top of canopy at noon	wg
Rad_l	–	W	Longwave radiation	Variable
Rad	–	W	Actual radiation	Variable
T_a	–	C	Actual air temperature	wg
t_{day}	–	h	Time of day	Variable
$T_{max,C}$	–	C	Maximum air temperature	wg
$T_{max,K}$	–	K	Maximum air temperature	wg
$T_{min,C}$	–	C	Minimum air temperature	wg
$T_{min,K}$	–	K	Minimum air temperature	wg
$t0$	–	h	Time of sunrise	Variable

Table A.3
Soil parameters.

Variable	Value	Unit	Description	Source
α	See Table 2	m	Soil physical parameter, van Genuchten	Carsel (1988)
ψ_s	–	Pa	Matric potential	Variable
θ_{sat}	See Table 2	–	Saturated soil moisture content	Carsel (1988)
θ_r	See Table 2	–	Residual soil moisture content	Carsel (1988)
θ	–	–	Soil moisture content	Variable
h_{gw}	–	m	Depth of groundwater	Variable
K_θ	–	m s^{-1}	Unsaturated conductivity	Variable
K_{sat}	See Table 2	m day^{-1}	Saturated conductivity	Carsel (1988)
m	$1-(1./n)$	–	Soil physical parameter, van Genuchten	van Genuchten (1980)
n	See Table 2	–	Soil physical parameter, van Genuchten	Carsel (1988)
Q_v	–	m s^{-1}	Vertical exchange flux between rootzone and groundwater	Variable
Z_r	0.6	m	Soil depth	This article

Table A.4
Vegetation parameters.

Variable	Value	Unit	Description	Source
α	0.5	–	Fraction reflected radiation	Friend (1995)
Γ^*	–	mol C mol^{-1} Air	CO_2 compensation point	Variable
γ_0	34.6e−6	mol mol^{-1}	CO_2 compensation point	Daly et al. (2004)
γ_1	0.0451	K^{-1}	Empirical constant for calculation of Γ	Daly et al. (2004)
γ_2	0.000347	K^{-2}	Empirical constant for calculation of Γ	Daly et al. (2004)
$\lambda_{sapwood}$	1	–	Sapwood fraction of total stem biomass	Variable
ψ_0	−4.5e6	Pa	Leaf water potential where g_s becomes 0	Daly et al. (2004)
ψ_1	−0.05e6	Pa	Leaf water potential where g_s begins to decline	Daly et al. (2004)
ψ_{a0}	−4.5e6	Pa	Leaf water potential where assimilation becomes 0	Daly et al. (2004)
ψ_{a1}	−0.5e6	Pa	Leaf water potential where assimilation begins to decline	Daly et al. (2004)
ψ_l	–	Pa	Leaf water potential	Variable
ρ_{stem}	350	kg m^{-3}	Wood density	Schwalm and Ek (2004)
a_{md}	0.1	–	Allometric scaling, tree dimension	Zianis and Radoglou (2006)
a_{nrtree}	30	–	Allometric scaling, number of trees	This article
a_{sw}	–	kg^{-1}	Parameter controlling sapwood area	This article
a	–	–	Parameter influencing RAI	Variable
An	–	mol m^{-2} s^{-1}	Carbon assimilation	Variable
$An_{\psi,l}$	–	–	Carbon assimilation reduction due to low Psi_l	Variable
An_{bio}	–	mol m^{-2} s^{-1}	Carbon assimilation based biochemical processes	Variable
An_{gsba}	–	mol m^{-2} s^{-1}	Carbon assimilation based on stomatal conductance	Variable
An_c	–	mol m^{-2} s^{-1}	Carbon assimilation based biochemical capacity, per unit leaf area	Variable
An_Q	–	mol m^{-2} s^{-1}	Carbon assimilation based on radiation, per unit leaf area	Variable

Table A.4 (Continued)

Variable	Value	Unit	Description	Source
$APAR$	–	W	Absorbed photosynthetic active radiation	Variable
AR_L	–	W	Absorbed radiation of layer L	Variable
B_{above}	–	kg	Aboveground biomass per cell	Variable
B_{lai}	–	kg	Biomass of LAI	Variable
B_{mol}	–	mol	Biomass per cell	Variable
b_{nrtree}	6900	–	Allometric scaling, number of trees	This article
B_{sw}	–	kg	Sapwood biomass	Variable
b_{tree}	2.5	–	Allometric scaling, tree dimension	Zianis and Radoglou (2006)
B_{tree}	–	kg	Biomass per tree	Variable
$C_{f,root}$	0.3	???	C fraction of root	Foley et al. (1996)
$C_{f,stem}$	0.3	???	C fraction of stem	Foley et al. (1996)
$C_{fraction}$	0.45	–	Carbon fraction of dry biomass	Ollinger and Smith (2005)
C_i	–	mol C mol^{-1} air	Intercellular carbon concentration	Variable
c_{nrtree}	0.43	–	Allometric scaling, number of trees	This article
c	2	–	Parameter of the vulnerability curve	Daly et al. (2004)
cn_{leaf}	29	–	Leaf C:N ratio	Sitch et al. (2003)
cn_{root}	29	–	Root C:N ratio	Sitch et al. (2003)
$cn_{sapwood}$	330	–	Sapwood C:N ratio	Sitch et al. (2003)
D_{stem}	–	m	Diameter of stem	Variable
$d_{z,crown,i}$	–	m	Thickness of canopy layer L for species i	Variable
d	2e6	Pa	Parameter of the vulnerability curve	Daly et al. (2004)
E_O	–	m s^{-1}	Open water evapotranspiration	Variable
ET_{pm}	–	m s^{-1}	Transpiration according to Penman–Monteith equation	Variable
f_{ψ_l}	–	–	Leaf water potential reduction function, for g_s	variable
f_{above}	0.8	–	Above ground biomass fraction	This article
f_D	–	–	Water vapor deficit reduction function, for g_s	Variable
f_{gap}	–	–	Canopy gap fraction	Variable
f_{ox}	–	–	Reduction function for oxygen stress	Variable
f_{Rad}	–	–	Radiation reduction function, for g_s	Variable
f_{store}	0.11	–	Fraction of sapwood for storage	Friend et al. (1997)
f_{Ta}	–	–	Air temperature reduction function, for g_s	Variable
g_{a,CO_2}	g_a/LAI	mol m^{-2} s^{-1}	Atmospheric conductance for CO_2	Jones in Daly et al. (2004)
g_a	0.02	m s^{-1}	Atmospheric conductance	Daly et al. (2004)
g_{b,CO_2}	$g_b/1.37$	mol m^{-2} s^{-1}	Leaf boundary layer conductance for CO_2	Jones in Daly et al. (2004)
g_b	0.02	m s^{-1}	Leaf boundary layer conductance	Daly et al. (2004)
g_{ba,CO_2}	–	mol m^{-2} s^{-1}	Conductance boundary layer atmosphere	Variable
$g_{p,max}$	11.7e−12	m Pa^{-1} s^{-1}	Maximum plant conductance	Daly et al. (2004)
g_{s,CO_2}	$g_s/1.6$	mol m^{-2} s^{-1}	Stomatal conductance for CO_2	Jones in Daly et al. (2004)
$g_{s,max}$	0.01	m s^{-1}	Maximum stomatal conductance	Breuer et al. (2003)
g_{sba,CO_2}	–	mol m^{-2} s^{-1}	Series of conductances for CO_2	Variable
g_{srp}	–	m Pa^{-1} s^{-1}	Soil root plant conductance	Variable
g_s	–		Stomatal conductance	Variable
H_{dJ}	2,01,000	J mol^{-1}	Deactivation energy for J_{max}	Daly et al. (2004)
H_{dV}	2,02,900	J mol^{-1}	The energy of deactivation	Daly et al. (2004)
H_{Kc}	59 430	J mol^{-1}	Activation energy for k_c	Daly et al. (2004)
H_{Ko}	36 000	J mol^{-1}	Activation energy for k_o	Daly et al. (2004)
H_{tree}	–	m	Height of tree	Variable
H_{vJ}	79 500	J mol^{-1}	Activation energy for J_{max}	Daly et al. (2004)
H_{vV}	1,16,300	J mol^{-1}	The energy of activation	Daly et al. (2004)
I_{cap}	0.0005	m	Interception capacity	This article
I_{max}	–	m s^{-1}	Maximum interception	Variable
J_{max}	–	mol m^{-2} s^{-1}	Electron flux	Variable
$J_{max,0}$	75e−6	mol electrons m^{-2} s^{-1}	Potential rate of whole-chain electron transport at T_0	Daly et al. (2004)
J	–	mol photons s^{-1} m^{-2}	Incident electron flux of APAR	Variable
K_{c0}	302e−6	mol mol^{-1}	Michaelis Menten constant for CO_2	Daly et al. (2004)
K_{o0}	0.256	mol mol^{-1}	Michaelis Menten constant for O_2	Daly et al. (2004)
k_1	0.95	–	Shape parameter for calculation of J_{max}	Daly et al. (2004)
k_1	0.005	m^2 W^{-1}	Radiation sensitivity constant for Jarvis	Daly et al. (2004)
k_2	0.0016	K^{-2}	Temperature sensitivity constant for Jarvis	Daly et al. (2004)
k_2	0.2	mol electrons mol^{-1} photons	Quantum yield of whole-chain electron transport at T_0 for calculation of J_{max}	Daly et al. (2004)
k	0.5	–	Light extinction coefficient	Jarvis and leverenz 1983 inWoodward et al. (1995)
LAD	–	m^{-1}	Leaf area density	Variable
LAI_d	0.1	m s^{-1}	LAI decline rate	This article
LAI_g	0.03	m s^{-1}	LAI growth rate	This article
$LAI_{L,i}$	–	–	LAI of canopy layer L for species I	Variable
LAI_L	–	–	LAI of canopy layer L	Variable
LAI_{max}	–	–	Maximum LAI given biomass	Variable
LAI	5.0	–	Leaf area index	Breuer et al. (2003)
M_{stem}	–	kg	Mass in stem	Variable
n_f	5000	m m^{-1}	Foliage to sapwood ratio	This article
N_{Tr}	–	–	Number of trees ha^{-1}	Variable
$OX1_\theta$	0.3	–	Soil moisture content where root water uptake begins to decline	This article
$OX2_\theta$	0.4	–	Soil moisture content where root water uptake becomes 0	This article
P_{ind}	–	m	Indirect precipitation, throughfall	Variable

Table A.4 (Continued)

Variable	Value	Unit	Description	Source
P_{int}	–	m	Interception	Variable
R_{growth}	$0.3 \times An$	mol m^{-2} s^{-1}	Growth respiration	Dufrêne et al. (2005)
R_{leaf}	$0.015 \times V_{cmax}$	mol m^{-2} s^{-1}	Leaf respiration	Variable
r	0.066	g C g N day^{-1}	Tissue respiration rate at 10 °C	Sitch et al. (2003)
RAI_{frac}	1.5	–	RAI–LAI fraction	This article
RAI	–	–	Root area index	Variable
S_v	650	J mol^{-1}	Entropy term	Daly et al. (2004)
S	–	mol	Carbon storage of tree	Variable
SLA	37	m^2 kg^{-1}	Specific leaf area	Zianis and Radoglou (2006)
T_0	−273	°C	Absolute minimum temperature	This article
T_0	293.2	K	Optimal temperature for carbon assimilation	Daly et al. (2004)
T_a	–	°C	Actual temperature	This article
T_l	–	K	Leaf temperature	Variable
T_{opt}	298	K	Optimal temperature of g_s for Jarvis	Daly et al. (2004)
T_{root}	10	°C	Temperature of root	This article
T_{stem}	10	°C	Temperature of stem	This article
T_{sum}	100	°C	Temperature sum leaf growth	This article
$\overline{T_{day}}$	–	°C	Mean day temperature	Variable
$\overline{T_{year}}$	–	°C	Mean year temperature	Variable
$V_{c,max}$	–	mol m^{-2} s^{-1}	Maximum carboxylation rate at T	Variable
V_{cmax0}	50e−6	mol m^{-2} s^{-1}	Maximum carboxylation rate at T_0	Daly et al. (2004)
V_{stem}	–	m^3	Volume of stem	Variable
Z_{sw}	–	m^2	Sapwood area at breast height	Variable

References

Allen, R., Pereira, L., Raes, D., Smith, M., 1998. Crop evapotranspiration. Guidelines for Computing Crop Water Requirements. Tech. Rep. 56, FAO.

Arora, V.K., 2002. Modeling vegetation as a dynamic component in soil–vegetation–atmosphere transfer schemes and hydrological models. Reviews of Geophysics 40 (2), 1–3.

Breuer, L., Eckhardt, K., Frede, H.-G., 2003. Plant parameter values for models in temperate climates. Ecological Modelling 169 (2–3), 237–293.

Brolsma, R., van Beek, R., Bierkens, M.F.P., 2010. Vegetation competition model for water, oxygen and light limitation. I. Influence of groundwater and spatial dynamics, Ecological Modelling.

Brolsma, R.J., Bierkens, M.F.P., 2007. Groundwater–soil water–vegetation dynamics in a temperate forest ecosystem along a slope. Water Resources Research 43 (1).

Carsel, R., 1988. Developing joint probability distributions of soil water retention characteristics. Water Resources Research 5 (5), 755–769.

Daly, E., Porporato, A., Rodriguez-Iturbe, I., 2004. Coupled dynamics of photosynthesis, transpiration, and soil water balance. Part I. Upscaling from hourly to daily level. Journal of Hydrometeorology 5 (3), 546–558.

Dufrêne, E., Davi, H., François, C., Le Maire, G., Le Dantec, V., Granier, A., 2005. Modelling carbon and water cycles in a beech forest. Part I. Model description and uncertainty analysis on modelled NEE. Ecological Modelling 185 (2–4), 407–436.

Farquhar, G.D., Von Caemmerer, S., Berry, J.A., 1980. A biochemical model of photosynthetic CO_2 assimilation in leaves of C3 species. Planta 149, 78–90.

Feddes, R.A., Kowalik, P., Jaradny, H., 1978. Simulation of field water use and crop yield. In: Simulation Monographs. Pudoc, Wageningen, p. 189.

Foley, J.A., Prentice, I.C., Ramankutty, N., Levis, S., Pollard, D., Sitch, S., Haxeltine, A., 1996. An integrated biosphere model of land surface processes, terrestrial carbon balance, and vegetation dynamics. Global Biogeochemical Cycles 10 (4), 603–628.

Friend, A.D., 1995. Pgen—an integrated model of leaf photosynthesis, transpiration, and conductance. Ecological Modelling 77 (2–3), 233–255.

Friend, A.D., 2001. Modelling canopy CO_2 fluxes: are 'big-leaf' simplifications justified? Global Ecology and Biogeography 10 (6), 603–619.

Friend, A.D., Stevens, A.K., Knox, R.G., Cannell, M.G.R., 1997. A process-based, terrestrial biosphere model of ecosystem dynamics (Hybrid v3.0). Ecological Modelling 95 (2–3), 249–287.

Jansen, J., Sevenster, J., Faber, P., 1996. Opbrengst tabellen voor belangrijke boomsoorten in Nederland. Tech. Rep. IBN 221.

Jarvis, P.G., 1976. The interpretation of the variations in leaf water potential and stomatal conductance found in canopies in the field. Philosophical Transactions Royal Society London 273, 593–610.

Katul, G., Leuning, R., Oren, R., 2003. Relationship between plant hydraulic and biochemical properties derived from a steady-state coupled water and carbon transport model. Plant, Cell and Environment 26 (3), 339–350.

Knohl, A., Schulze, E.D., Kolle, O., Buchmann, N., 2003. Large carbon uptake by an unmanaged 250-year-old deciduous forest in central Germany. Agricultural and Forest Meteorology 118 (3–4), 151–167.

Landsberg, J., 1986. Physiological Ecology of Forest Production, vol. XVIII. Academic Press.

Leuning, R., 1990. Modelling stomatal behaviour and photosynthesis of eucalyptus grandis. Australian Journal of Plant Physiology 17, 159–175.

Leuning, R., 1995. A critical appraisal of a combined stomatal-photosynthesis model for c3 plants. Plant, Cell and Environment 18 (4), 339–355.

Monteith, J.L., 1965. Evaporation and environment. Symposia of the Society for Experimental Biology 19, 205–234.

Ollinger, S.V., Smith, M.L., 2005. Net primary production and canopy nitrogen in a temperate forest landscape: an analysis using imaging spectroscopy, modeling and field data. Ecosystems 8 (7), 760–778.

Parton, W.J., 1993. Observations and modeling of biomass and soil organic matter dynamics for the grassland biome worldwide. Global Biogeochemical Cycles 7 (4), 785–809.

Potter, C.S., 1993. Terrestrial ecosystem production: a process model based on global satellite and surface data. Global Biogeochemical Cycles 7 (4), 811–841.

Richardson, C., 1981. Stochastic simulation of daily precipitation, temperature, and solar radiation. Water Resources Research 17 (1), 182–190.

Rodriguez-Iturbe, I., D'Odorico, P., Laio, F., Ridolfi, L., Tamea, S., 2007. Challenges in humid land ecohydrology: interactions of water table and unsaturated zone with climate, soil, and vegetation. Water Resources Research 43 (9).

Running, S.W., Coughlan, J.C., 1988. A general-model of forest ecosystem processes for regional applications. 1. Hydrologic balance, canopy gas-exchange and primary production processes. Ecological Modelling 42 (2), 125–154.

Ryan, M.G., 1991. Effects of climate change on plant respiration. Ecological Applications 1 (2), 157–167.

Schaap, M.G., Leij, F.J., Van Genuchten, M.T., 1998. Neural network analysis for hierarchical prediction of soil hydraulic properties. Soil Science Society of America Journal 62 (4), 847–855.

Schwalm, C.R., Ek, A.R., 2004. A process-based model of forest ecosystems driven by meteorology. Ecological Modelling 179 (3), 317–348.

Shuttleworth, W., 1993. Evaporation. In: Maidment, D. (Ed.), Handbook of Hydrology. McGraw-Hill, New York, pp. 4.1–4.53.

Sitch, S., Smith, B., Prentice, I.C., Arneth, A., Bondeau, A., Cramer, W., Kaplan, J.O., Levis, S., Lucht, W., Sykes, M.T., Thonicke, K., Venevsky, S., 2003. Evaluation of ecosystem dynamics, plant geography and terrestrial carbon cycling in the LPJ dynamic global vegetation model. Global Change Biology 9 (2), 161–185.

Sprugel, D.G., Ryan, M.G., Brooks, J.R., Vogt, K.A., Martin, T.A., 1995. Respiration from the organ level to the stand. In: Smith, W.K., Hinckley, T.M. (Eds.), Resource Physiology of Conifers. Academic Press Inc., San Diego, pp. 255–299.

Teuling, A.J., Troch, P.A., 2005. Improved understanding of soil moisture variability dynamics. Geophysical Research Letters 32 (5).

van Genuchten, M.T., 1980. A closed-form equation for predicting the hydraulic conductivity of unsaturated soils. Soil Science Society America Journal 44, 892–898.

Woodward, F.I., Smith, T.M., Emanuel, W.R., 1995. A global land primary productivity and phytogeography model. Global Biogeochemical Cycles 9 (4), 471–490.

Zavala, M.A., 2004. Integration of drought tolerance mechanisms in Mediterranean sclerophylls: a functional interpretation of leaf gas exchange simulators. Ecological Modelling 176 (3–4), 211–226.

Zianis, D., Radoglou, K., 2006. Comparison between empirical and theoretical biomass allometric models and statistical implications for stem volume predictions. Forestry 79 (4), 477–487.